# Pliniusite, $Ca_5(VO_4)_3F$, a new apatite-group mineral and the novel natural ternary solid-solution system pliniusite–svabite–fluorapatite

Igor V. Pekov[1]*, Natalia N. Koshlyakova[1], Natalia V. Zubkova[1], Arkadiusz Krzątała[2], Dmitry I. Belakovskiy[3], Irina O. Galuskina[2], Evgeny V. Galuskin[2], Sergey N. Britvin[4], Evgeny G. Sidorov[5†], Yevgeny Vapnik[6] and Dmitry Yu. Pushcharovsky[1]

[1]Faculty of Geology, Moscow State University, Vorobievy Gory, 119991 Moscow, Russia

[2]Institute of Earth Sciences, Faculty of Natural Sciences, University of Silesia, Będzińska 60, 41-200 Sosnowiec, Poland

[3]Fersman Mineralogical Museum of the Russian Academy of Sciences, Leninsky Prospekt 18-2, 119071 Moscow, Russia

[4]Department of Crystallography, St. Petersburg State University, University Emb. 7/9, 199034 St. Petersburg, Russia

[5]Institute of Volcanology and Seismology, Far Eastern Branch of Russian Academy of Sciences, Piip Boulevard 9, 683006 Petropavlovsk-Kamchatsky, Russia

[6]Department of Geological and Environmental Sciences, Ben-Gurion University of the Negev, POB 653, Beer-Sheva 84105, Israel

† Deceased 20 March 2021

*Corresponding author: igorpekov@mail.ru

This is the peer-reviewed, final accepted version for American Mineralogist, published by the Mineralogical Society of America.
The published version is subject to change. Cite as Authors (Year) Title. American Mineralogist, in press.
DOI: https://doi.org/10.2138/am-2022-8100. http://www.minsocam.org/

## ABSTRACT

The new apatite-group mineral pliniusite, ideally $Ca_5(VO_4)_3F$, was found in fumarole deposits at the Tolbachik volcano (Kamchatka, Russia) and in a pyrometamorphic rock of the Hatrurim Complex (Israel). Pliniusite, together with fluorapatite and svabite, forms a novel and almost continuous ternary solid-solution system characterized by wide variations of $T^{5+}$ = P, As and V. In paleo-fumarolic deposits at Mountain 1004 (Tolbachik), members of this system, including the holotype pliniusite, are associated with hematite, tenorite, diopside, andradite, kainotropite, baryte and supergene volborthite, brochantite, gypsum and opal. In sublimates of the active Arsenatnaya fumarole (Tolbachik), pliniusite–svabite–fluorapatite minerals occur with anhydrite, diopside, hematite, berzeliite, schäferite, calciojohillerite, forsterite, enstatite, magnesioferrite, ludwigite, rhabdoborite-group fluoroborates, powellite, baryte, udinaite, arsenudinaite, paraberzeliite, and spinel. At Nahal Morag, Negev Desert, Israel, the pliniusite cotype and V-bearing fluorapatite occur in schorlomite-gehlenite paralava with rankinite, walstromite, zadovite-aradite series minerals, magnesioferrite, hematite, khesinite, barioferrite, perovskite, gurimite, baryte, tenorite, delafossite, wollastonite and cuspidine. Pliniusite forms hexagonal prismatic crystals up to 0.3 mm × 0.1 mm and open-work aggregates up to 2 mm across (Mountain 1004) or grains up to 0.02 mm (Nahal Morag and Arsenatnaya fumarole). Pliniusite is transparent to semitransparent, colorless or whitish, with vitreous lustre. The calculated density is 3.402 g cm$^{-3}$. Pliniusite is optically uniaxial (–), $\omega$ = 1.763(5), $\varepsilon$ = 1.738(5). The empirical formulae of pliniusite type specimens calculated based on 13 anions (O+F+Cl) per formula unit are $(Ca_{4.87}Na_{0.06}Sr_{0.03}Fe_{0.02})_{\Sigma 4.98}(V_{1.69}As_{0.66}P_{0.45}S_{0.12}Si_{0.09})_{\Sigma 3.01}O_{11.97}F_{1.03}$ (Mountain 1004) and $(Ca_{4.81}Sr_{0.12}Ba_{0.08}Na_{0.05})_{\Sigma 5.06}(V_{2.64}P_{0.27}S_{0.07}Si_{0.03})_{\Sigma 3.01}O_{12.15}F_{0.51}Cl_{0.34}$ (Nahal Morag). Pliniusite has a hexagonal structure with space group $P6_3/m$, $a = b = 9.5777(7)$, $c = 6.9659(5)$ Å, $V = 553.39(7)$ Å$^3$ and $Z = 2$. The structure was solved using single-crystal (holotype) X-ray diffraction, $R = 0.0254$. The mineral was named in honor of the famous Roman naturalist Pliny the Elder, born Gaius Plinius

53 Secundus (AD 23–79). It is suggested that the combination of high temperature, low pressure and
54 high oxygen fugacity favors the incorporation of $V^{5+}$ into calcium apatite-type compounds, leading
55 to the formation of fluorovanadates.
56
57 **Keywords**: pliniusite, apatite group, new mineral, calcium fluoride vanadate, fluorapatite,
58 svabite, crystal structure, fumarole sublimate, pyrometamorphic rock, Tolbachik volcano, Hatrurim
59 Complex
60

This is the peer-reviewed, final accepted version for American Mineralogist, published by the Mineralogical Society of America.
The published version is subject to change. Cite as Authors (Year) Title. American Mineralogist, in press.
DOI: https://doi.org/10.2138/am-2022-8100. http://www.minsocam.org/

61

62 ## INTRODUCTION

63

64 The family of apatite-type compounds (apatites, in the common chemical terminology) is
65 huge. It includes more than forty natural members, valid mineral species belonging to the apatite
66 supergroup, and several hundred synthetic phases. This family is well-known and does not need a
67 special presentation, as well as the importance of apatites in natural sciences, modern technologies
68 and human life in general (Kohn et al. 2002).

69 The general simplified formula of apatites is $M_5(TO_4)_3X$ and the crystal chemical formula is
70 $^{IX}M1_2{}^{VII}M2_3(^{IV}TO_4)_3X$ ($Z = 2$), where the Roman numerals indicate the ideal coordination numbers.
71 Apatite-type compounds are hexagonal or pseudo-hexagonal. The space group of the archetype
72 structure of apatite is $P6_3/m$. In minerals of the apatite supergroup, the following components are
73 now known as the species-defining ones: $M = Ca^{2+}$, $Sr^{2+}$, $Ba^{2+}$, $Pb^{2+}$, $Mn^{2+}$, $Cd^{2+}$, $Na^{+}$, $Y^{3+}$, $La^{3+}$,
74 $Ce^{3+}$, $Nd^{3+}$, $Bi^{3+}$; $T = P^{5+}$, $As^{5+}$, $V^{5+}$, $Si^{4+}$, $S^{6+}$, $B^{3+}$; $X = F^{-}$, $(OH)^{-}$, $Cl^{-}$, $O^{2-}$ (Pasero et al. 2010; The
75 New IMA List... 2021). Based on both chemical and crystal chemical (first of all, ordering of metal
76 cations between different $M$ sites) criteria, five groups have been distinguished within the apatite
77 supergroup: apatite group, hedyphane group, belovite group, britholite group, and ellestadite group.
78 The most widespread in nature and the most numerous apatite-supergroup members belong to the
79 apatite group which includes minerals with pentavalent $T$ constituents ($T^{5+}$ = P, As or V) containing
80 the same prevailing (species-defining) bivalent cation at both the $M1$ and $M2$ sites (Pasero et al.
81 2010).

82 Phosphates and arsenates are the most diverse among apatite-supergroup minerals. In
83 contrast, natural apatite-type vanadates before recently were represented by the only species
84 vanadinite $Pb_5(VO_4)_3Cl$, a member of the apatite group (The New IMA List... 2021). In this paper
85 we describe the second natural apatite-supergroup vanadate, **pliniusite**, ideally $Ca_5(VO_4)_3F$. This

new mineral belonging, like vanadinite, to the apatite group, originates from fumaroles of the Tolbachik volcano (Kamchatka, Russia) and from pyrometamorphic rocks of the Hatrurim Complex (Israel).

Pliniusite (Cyrillic: плиниусит) was named in honor of the famous Roman naturalist, natural philosopher, author and statesman Pliny the Elder, born Gaius Plinius Secundus (AD 23–79), who wrote the encyclopedic *Naturalis Historia*, which became, in fact, a model for encyclopedias in general. He observed the famous eruption of the Vesuvius volcano in 79 AD and died as a victim of this catastrophic eruption; this kind of volcanic eruptions was named in his memory a Plinian eruption. It is worthy to note that the holotype pliniusite was formed at the Tolbachik volcano during or immediately after the ancient eruption happened about two thousand years ago, approximately in the same time when Pliny the Elder lived.

Both the new mineral and its name have been approved by the Commission on New Minerals, Nomenclature and Classification of the International Mineralogical Association (IMA No. 2018–031). The type specimens are deposited in the systematic collection of the Fersman Mineralogical Museum of the Russian Academy of Sciences, Moscow under the catalogue numbers 96261 (Tolbachik) and 96262 (Hatrurim).

Vanadium is an exotic constituent in the majority of apatite-supergroup minerals, whereas many synthetic apatites with various $V^{5+}$ contents at the *T* site are known (White et al. 2005). In this light, we considered of interest to characterize the novel ternary solid-solution system between fluorapatite $Ca_5(PO_4)_3F$, svabite $Ca_5(AsO_4)_3F$ and pliniusite with wide variations of the tetrahedrally coordinated constituents $T^{5+}$ = P, As and V.

## ANALYTICAL METHODS

The chemical composition of the minerals was determined by electron microprobe in two laboratories. The chemical data for samples from Tolbachik were obtained in the Laboratory of Analytical Techniques of High Spatial Resolution, Dept. of Petrology, Moscow State University (MSU) using a Jeol JSM-6480LV scanning electron microscope equipped with an INCA-Wave 500 wavelength-dispersive spectrometer, with an acceleration voltage of 20 kV, a beam current of 20 nA, and a 3 μm beam diameter. Pliniusite from Hatrurim was examined at the Institute of Geochemistry, Mineralogy and Petrology, University of Warsaw (UW) using a Cameca SX100 instrument (WDS mode, 15 kV, 10 nA, 1 μm beam diameter). The reference materials used are as follows (MSU / UW): Na (jadeite / albite), K ($KTiOPO_4$ / orthoclase), Ca ($CaSiO_3$ / diopside), Fe ($FeS_2$ / $Fe_2O_3$), Sr ($SrSO_4$ / $SrSO_4$), Ba ($BaSO_4$ / $BaSO_4$), Si (jadeite / diopside), P ($KTiOPO_4$ / $Ca_5P_3O_{12}F$), V (V / $V_2O_5$), As (GaAs / GaAs), S (ZnS / $BaSO_4$), F ($MgF_2$ / $Ca_5P_3O_{12}F$), and Cl (NaCl / tugtupite). Contents of other elements with atomic numbers higher than that of carbon are below detection limits.

The electron microscopic studies of Tolbachik samples were carried out using the same scanning electron microscope at MSU. The samples from Hatrurim were studied using a Phenom XL scanning electron microscope, Faculty of Earth Sciences, University of Silesia, Sosnowiec, Poland.

Raman spectra of pliniusite from both localities were collected using a WITec alpha 300R Confocal Raman Microscope (Department of Earth Science, University of Silesia) equipped with an air-cooled solid-state laser (532 nm) and a CCD camera operating at –61°C. An air Zeiss LD EC Epiplan-Neofluan DIC-100/0.75NA objective was used. Raman scattered light was focused on a broadband single-mode fibre with an effective pinhole size of about 30 μm. A monochromator with a 600 gr $mm^{-1}$ grating was used, and the resolution was 3 $cm^{-1}$. The power of the laser at the sample position was *ca*. 30 mW. Integration times of 3 s with an accumulation of 30 scans were chosen. The monochromator was calibrated using the Raman scattering line of a silicon plate (520.7 $cm^{-1}$).

This is the peer-reviewed, final accepted version for American Mineralogist, published by the Mineralogical Society of America.
The published version is subject to change. Cite as Authors (Year) Title. American Mineralogist, in press.
DOI: https://doi.org/10.2138/am-2022-8100. http://www.minsocam.org/

Spectra processing such as baseline correction and smoothing was performed using the SpectraCalc software package GRAMS (Galactic Industries Corporation, NH, USA). The fitting of Raman spectra was performed using a Gauss and Lorentz cross-product function, with a minimum number of component bands used for the fitting process.

Powder X-ray diffraction (XRD) of the holotype pliniusite was carried out using a Rigaku R-AXIS Rapid II single-crystal diffractometer equipped with a curved image plate detector (Debye-Scherrer geometry, $r$ = 127.4 mm) and Co$K\alpha$ radiation source (rotating anode, 40 kV, 15 mA), with Rigaku VariMax microfocus mirror optics. Imaging plate-to-profile data conversion was performed using osc2xrd software (Britvin et al. 2017).

Single-crystal XRD of the holotype pliniusite was carried out using an Xcalibur S CCD diffractometer (Mo$K\alpha$ radiation). A full sphere of three-dimensional data was collected. Data reduction was performed using CrysAlisPro Version 1.171.37.35 (Agilent et al. 2014). The data were corrected for Lorentz and polarization effects. The structure was solved by direct methods and refined with the use of SHELX software package (Sheldrick 2008) on the basis of 416 independent reflections with $I > 2\sigma(I)$ to $R$ = 0.0254 in the frame of space group $P6_3/m$. Trials to lower the symmetry to $P6_3$, $P2_1/m$ or $P$-1 (two latter space groups were reported for synthetic vanadate apatites: see below) did not result in any improvement of the structural model and the $R$ value increased in all these cases. A complete set of crystallographic data can be retrieved from the CIF file attached as the Supplementary Material.

## RESULTS AND DISCUSSION

### Occurrence and mineral associations

The holotype of pliniusite originates from the Tolbachik volcano. This material was collected in July 2017 from paleo-fumarolic deposits of the Southern fumarole field at Mountain 1004, a scoria cone located 20 km SSW of the active volcano Ploskiy Tolbachik. Mountain 1004 is a

monogenetic volcano formed as a result of an ancient eruption of Tolbachik, approximately two thousand years ago (Fedotov and Markhinin 1983). All fumaroles at Mountain 1004 are extinct; however, some water-insoluble sublimate minerals are well-preserved to date. The members of the pliniusite–svabite–fluorapatite solid-solution system are associated here with hematite, tenorite, diopside, andradite, kainotropite, and baryte. The secondary mineralization, formed as a result of the supergene alteration of unstable sublimate minerals, is represented by volborthite, brochantite, gypsum and opal.

In 2018, pliniusite and V-rich varieties of svabite and fluorapatite were found in the active Arsenatnaya fumarole located at the Second scoria cone of the Northern Breakthrough of the Great Tolbachik Fissure Eruption of 1975–1976. This scoria cone is a monogenetic volcano formed in 1975. It is situated 2 km north of Mountain 1004 and demonstrates strong fumarole activity at present day. The Arsenatnaya fumarole is one of the most mineralogically interesting fumaroles at the Tolbachik volcano and, in general, one of the brightest representatives of strongly mineralized oxidizing-type fumaroles in the world. From the mineralogical point of view, this fumarole was characterized, including the data on zonation in distribution of mineral associations, by Pekov et al. (2018) and Shchipalkina et al. (2020). Minerals of the pliniusite–svabite–fluorapatite solid-solution system were found in the deepest and hottest zone of the Arsenatnaya fumarole. It is located at the depth of 3–4 m under day surface; temperatures in the pockets with these minerals measured by us using a chromel-alumel thermocouple were 450–490°C. The associated minerals include anhydrite, diopside, hematite, berzeliite, schäferite, calciojohillerite and subordinate forsterite, enstatite, magnesioferrite, ludwigite, rhabdoborite-group fluoroborates, powellite, baryte, wagnerite (As-bearing variety), udinaite, arsenudinaite, paraberzeliite, and spinel.

The cotype material of pliniusite originates from the Nahal Morag canyon area, about 10 km southeast of Arad city, Negev Desert, Israel. The new mineral occurs in pyrometamorphic rocks belonging to the Hatrurim Basin, which is one of the largest unit of the Hatrurim Complex. It is

generally recognised that terrigenous-carbonate protolith of the Hatrurim Complex was driven by combustion processes. The geology and origin of the Hatrurim Complex have been discussed previously in detail (Gross 1977; Burg et al. 1999; Novikov et al. 2013; Galuskina et al. 2014). The Nahal Morag canyon crosscuts the central part of the Hatrurim Basin from west to east. In its eastern part there are several cliff-like outcrops (up to 10 m across and up to 1 m in height) of gehlenite-bearing rocks rising along the borders of Nahal Morag. At least in part of them coarse-grained veins (typically 1–3 cm thick) of paralavas occur. Pliniusite was found in vein-like bodies of schorlomite-gehlenite paralava hosted by melilite hornfels. The assemblage of major minerals of the paralavas includes melilite of the gehlenite-alumoåkermanite series, garnet of the andradite-schorlomite series, rankinite, fluorapatite, walstromite, minerals of the zadovite-aradite series, magnesioferrite, hematite, khesinite, barioferrite, and $Fe^{3+}$-enriched perovskite. Pliniusite is typically confined to small oval polymineralic inclusions in rankinite and closely associated with gurimite, baryte, walstromite, tenorite, delafossite, wollastonite, cuspidine and secondary Ca hydrosilicates.

**General appearance, physical properties and optical data of pliniusite**

At Mountain 1004 (Tolbachik), pliniusite and vanadium-bearing varieties of svabite and fluorapatite, which are visually indistinguishable, occur as hexagonal prismatic (from long- to short-prismatic, equant), usually distorted and/or skeletal, cavernous crystals up to 0.3 mm long and up to 0.05 mm (rarely up to 0.1 mm) thick. Crystals are isolated or, more commonly, form near-parallel or chaotic clusters (Fig. 1) that are typically combined into open-work aggregates (Fig. 2) up to 2 mm across. These crystals overgrow hematite crusts which cover the surface of the basalt scoria altered by fumarolic gases. In some samples, members of the pliniusite–svabite–fluorapatite solid-solution system occur on diopside aggregates or directly on basaltic scoria. The major forms of pliniusite crystals from Mountain 1004 are the hexagonal prism {10-10} and the hexagonal bipyramid {10-11}; the pinacoid {0001} is common but subordinate and the hexagonal bipyramid {11-21} is minor

and rare. Some crystals are zoned, with a pliniusite core and svabite peripheral parts, or with a fluorapatite core and a pliniusite rim.

At the Arsenatnaya fumarole (Tolbachik), pliniusite and V-rich varieties of svabite and fluorapatite occur inside sublimate incrustations mainly consisting of anhydrite, diopside, hematite, garnets of the berzeliite–schäferite series, calciojohillerite, and V-poor svabite. Pliniusite forms grains up to 0.02 mm.

In coarse-grained paralava at Nahal Morag (Hatrurim), pliniusite typically occurs in polymineralic inclusions in rankinite (Figs. 3A and 3B). The new mineral forms grains commonly not exceeding 15 μm in size; rarely, its elongated prismatic crystals up to 40 μm in length are observed (Fig. 3C).

Pliniusite is transparent to semitransparent, colorless or whitish, with white streak and vitreous lustre. It does not fluoresce in ultraviolet light. Pliniusite is brittle, has (100) imperfect cleavage (as observed under microscope), and its fracture is uneven. The Vickers microhardness HVIT is 511 kg $mm^{-2}$ [mean of 3 measurements, min = 490, max = 530 kg $mm^{-2}$; max load: 20.00 mN; the Nanoindentation Tester ($NHT^3$) Anton-Paar was used], which corresponds to *ca*. 5 in the Mohs hardness scale. Density could not be measured because crystals are small and typically cavernous and aggregates are open-work. Density calculated for the holotype, using the empirical formula and unit-cell volume determined from the single-crystal XRD data, is 3.402 g $cm^{-3}$.

Under a plane polarized light microscope, pliniusite (the holotype) is colourless and non-pleochroic. It is optically uniaxial (–), $\omega$ = 1.763(5) and $\varepsilon$ = 1.738(5) (589 nm). Elongation is negative.

**Chemical composition**

Representative electron-microprobe analyses of minerals of the pliniusite–svabite–fluorapatite solid-solution system from Tolbachik fumaroles and pyrometamorphic rocks of Nahal

Morag are given in Table 1. The empirical formulae are calculated on the basis of 13 anions (O+F+Cl) per formula unit.

Calcium strongly prevails among *M* cations in these minerals with > 4.7 Ca atoms per formula unit (*apfu*). The major admixed *M* cations are Sr and Ba in samples from Nahal Morag (*ca*. 0.1 *apfu*: an. 2 and 3 in Table 1) and Na in samples from the Arsenatnaya fumarole (0.10–0.16 *apfu*: an. 13, 15, 17 and 19 in Table 1).

The F:Cl ratio significantly varies in minerals from the Arsenatnaya fumarole and Nahal Morag whereas the samples from Mountain 1004 are the F-richest and practically Cl-free.

The most interesting chemical feature of the studied minerals is their wide variations in ratios of the major tetrahedrally coordinated constituents $T^{5+}$ = V, P and As, based on 270 electron-microprobe analyses (Fig. 4). The V-richest samples originate from Nahal Morag (an. 2 in Table 1). At this locality, only As-free pliniusite and fluorapatite were found. In contrast, all studied samples from Tolbachik fumaroles contain As. The V:As:P ratios in Tolbachik samples vary widely, and in some samples the contents of the three *T* constituents are comparable (an. 5 and 6 in Table 1; Fig. 4). In general, the natural ternary solid-solution system among fumarolic fluorapatite, svabite and pliniusite is close to being continuous (Fig. 4).

Some samples from all three localities contain distinct amounts of admixed Si and S which sometimes demonstrate coupled substitutions according to the so-called ellestadite scheme: $Si^{4+} + S^{6+} \rightarrow 2T^{5+}$ (up to 0.8 Si+S *apfu*: no. 16 in Table 1).

The empirical formulae of two type specimens of pliniusite are as follows:

holotype (Mountain 1004, Tolbachik: no. 1 in Table 1):

$(Ca_{4.87}Na_{0.06}Sr_{0.03}Fe_{0.02})_{\Sigma 4.98}(V_{1.69}As_{0.66}P_{0.45}S_{0.12}Si_{0.09})_{\Sigma 3.01}O_{11.97}F_{1.03}$;

cotype (Nahal Morag, Hatrurim Basin: #2 in Table 1):

$(Ca_{4.81}Sr_{0.12}Ba_{0.08}Na_{0.05})_{\Sigma 5.06}(V_{2.64}P_{0.27}S_{0.07}Si_{0.03})_{\Sigma 3.01}O_{12.15}F_{0.51}Cl_{0.34}$.

The idealized, end-member formula of pliniusite is $Ca_5(VO_4)_3F$, which has CaO 49.70, $V_2O_5$ 48.35, F 3.37, O=F –1.42, total 100 wt%.

**Raman spectroscopy**

In the Raman spectra of pliniusite (Fig. 5) the main bands are related to vibrations of the $VO_4^{3-}$, $PO_4^{3-}$, $SO_4^{2-}$, $AsO_4^{3-}$ groups. The bands assigned to symmetric ($\nu_1$) and asymmetric ($\nu_3$) stretching vibrations of tetrahedral groups are above 750 $cm^{-1}$. Bands related to bending vibrations ($\nu_2$ and $\nu_4$) occur in the range 300-700 $cm^{-1}$. Bands below 300 $cm^{-1}$ can be assigned to lattice vibrations. The main bands in the Raman spectrum of pliniusite from Nahal Morag and their assignments are [$cm^{-1}$]: 204, 227 (lattice modes), 350 ($\nu_2$ $VO_4^{-3}$), 390 ($\nu_4$ $VO_4^{-3}$), 804, 831 ($\nu_3$ $VO_4^{-3}$) 850, 868, 881 ($\nu_1$ $VO_4^{-3}$), 955 ($\nu_1$ $PO_4^{-3}$), 1000 ($\nu_1$ $SO_4^{-2}$) (Frost et al. 2010; Comodi et al. 1999; Galuskin et al. 2015). The Raman spectrum of pliniusite from Mountain 1004 (Tolbachik) shows additional bands that can be assigned to arsenate and phosphate groups at 455 $cm^{-1}$ ($\nu_2$ $AsO_4^{-3}$), 575 $cm^{-1}$ ($\nu_4$ $PO_4^{3-}$), 859 $cm^{-1}$ ($\nu_1$ $AsO_4^{3-}$) and 1030 $cm^{-1}$ ($\nu_3$ $PO_4^{3-}$). Accurate bands assignment in the Raman spectra of pliniusite from Tolbachik is hampered by overlapping bands corresponding to vibrations of $VO_4^{3-}$, $AsO_4^{3-}$, $PO_4^{3-}$ and $SiO_4^{4-}$. The bands at 424 $cm^{-1}$ can be attributed to symmetric bending vibrations ($\nu_2$) of $AsO_4^{3-}$ or $\nu_2$ $PO_4^{3-}$ (Comodi et al. 1999; Frost et al. 2015). The absence or very low content of OH groups in pliniusite from both localities are confirmed by Raman spectroscopic data: bands in the region of 3600 – 3700 $cm^{-1}$ are absent.

**X-ray diffraction data and crystal structure of pliniusite**

Powder XRD data of the holotype pliniusite are given in Table 2. Unit-cell parameters of pliniusite obtained from powder data are: $a$ = 9.618(1), $c$ = 6.978(1) Å and $V$ = 559.0(2) $Å^3$. In comparison, those from single-crystal XRD data are: $a$ = 9.5777(7), $c$ = 6.9659(5) Å and $V$ = 553.39(7) $Å^3$.

This is the peer-reviewed, final accepted version for American Mineralogist, published by the Mineralogical Society of America.
The published version is subject to change. Cite as Authors (Year) Title. American Mineralogist, in press.
DOI: https://doi.org/10.2138/am-2022-8100. http://www.minsocam.org/

Although the apatite structure archetype is hexagonal, $P6_3/m$ (Pasero et al. 2010), cation ordering and/or topological distortions can reduce the symmetry. The synthetic compound with the idealized formula $Ca_5(VO_4)_3F$ demonstrates symmetry variations. The hexagonal ($P6_3/m$) form (Aia and Lublin 1966; White et al. 2005) is isostructural with other "ordinary" apatites. Dong and White (2004) reported monoclinic distortion and space group $P2_1/m$ for $Ca_{10}(VO_4)_6(F_{0.90}O_{0.05}\square_{0.05})_2$. Baikie et al. (2007) determined space group $P$-1 for $Ca_5(VO_4)_3F$ in which the symmetry lowering is caused by the tilting of $VO_4$ tetrahedra.

To check the symmetry of pliniusite (holotype), we tried to solve and refine its structure in space group $P$-1 and obtained the following unit-cell parameters: $a$ = 9.5750(8), $b$ = 9.5767(12), $c$ = 6.9645(5) Å, $\alpha$ = 90.039(8), $\beta$ = 89.981(6) and $\gamma$ = 119.956(10)°. Baikie et al. (2007) reported for synthetic triclinic $Ca_5(VO_4)_3F$ the following unit-cell data: $a$ = 9.6987(3), $b$ = 9.6933(3), $c$ = 7.0170(2) Å, $\alpha$ = 90.637(3), $\beta$ = 89.172(3) and $\gamma$ = 120.136(2)°. Thus, the deviations of parameters of the synthetic compound from the hexagonal cell are significantly greater than those for pliniusite. The $T$ position in the hexagonal structure of pliniusite transforms to three crystallographically non-equivalent sites in the triclinic model. However, they have site occupancy factors ( s.o.f.) [0.959(3), 0.954(3) and 0.963(3); vanadium scattering curve is used] and average $T$–O distances [1.631, 1.634 and 1.630 Å, respectively], compared with a $T$ s.o.f. of 0.956(3) ($e_{ref}$ = 21.99) and an average $T$–O distance of 1.631 Å in the hexagonal model (Table 3). Thus, the three $TO_4$ tetrahedra in the triclinic model are equivalent in both occupancy and dimensions. In addition, tetrahedral tilting was not found in this model.

Kreidler and Hummel (1970) reported the splitting of reflections (111), (211), (202) and (213) (indices are given for the hexagonal setting) in the powder XRD pattern of synthetic $Ca_5(VO_4)_3F$ as an indicator of the symmetry lowering from hexagonal to monoclinic. Our powder XRD pattern of pliniusite (Table 2) does not demonstrate such splitting.

This is the peer-reviewed, final accepted version for American Mineralogist, published by the Mineralogical Society of America.
The published version is subject to change. Cite as Authors (Year) Title. American Mineralogist, in press.
DOI: https://doi.org/10.2138/am-2022-8100. http://www.minsocam.org/

Thus, there is no sign of a symmetry lower than hexagonal for pliniusite, and we assume it adopts space group $P6_3/m$, the most typical structure for apatite-group members.

The basic features of the crystal structure of pliniusite (Fig. 6) are common to minerals of the apatite group (Pasero et al. 2010). Calcium cations occupy two sites with different coordination numbers: nine-fold polyhedron (6+3) is centered by *Ca*1 (Wyckoff position 4*f*) and seven-fold polyhedron (6+1) by *Ca*2 (6*h*). For the *T*(*V*) site the refined number of electrons is 21.99. This is in a good agreement with the chemical composition of the holotype specimen (Table 1). *Ca*1-centred polyhedra share faces to form columns running along the *c* axis. Adjacent columns are linked by $TO_4$ tetrahedra, thus forming a quasi-framework with the channels along the *c* axis (White et al. 2005) which host *Ca*2 sites in seven-fold coordination and $F^-$ anions located in the centre of the channels in symmetry plane at $z = 0.25$.

## Conditions of pliniusite formation

At the Tolbachik volcano, members of the pliniusite–svabite–fluorapatite solid-solution system are fumarolic minerals deposited directly from the gas phase as volcanic sublimates or formed as a result of the interaction between volcanic gas (as an obvious source of V, As, F and Cl) and basalt scoria. The latter way seems more probable taking into account low volatility of Ca in volcanic gases (Symonds and Reed 1993). These minerals crystallized in fumaroles belonging to the oxidizing type in which hot volcanic gas is mixed with atmospheric air that causes high oxygen fugacity (Africano et al. 2005). For active Tolbachik fumaroles it is concluded in the result of both direct determination of gas composition and detailed studies of sublimate minerals (Meniaylov et al. 1980; Zelenski et al. 2011; Pekov et al. 2020 and references therein). In the Arsenatnaya fumarole, minerals of the pliniusite–svabite–fluorapatite solid-solution system crystallized at temperatures not lower than 500°C and, based on data published by Meniaylov et al. (1980), not higher than 800°C.

The mineral assemblage observed in paleo-fumarolic deposits at the Southern fumarole field of Mountain 1004 allows us to suggest the same or similar conditions of formation.

At Nahal Morag, the formation of pliniusite in schorlomite-gehlenite paralava (Fig. 3A), which forms veinlets in gehlenite hornfels, is related to the formation of small portions of Ba-, Ti-, P-, V-, Cu-, U- and F-enriched residual melts. This melt, remained after the relatively rapid crystallization of rock-forming minerals of the paralava, gave the specific polymineralic enclaves in rankinite (Fig. 3B) or in interstices between gehlenite and schorlomite crystals (Krzątała et al. 2020). Pliniusite is associated here with Ba- and/or V-bearing minerals, e.g., walstromite $BaCa_2(Si_3O_9)$ and gurimite, $Ba_3(VO_4)_2$ (Fig. 3C), and it is Ba-richer, compared to fumarolic pliniusite from Tolbachik, and is As-free as well (Table 1). The presence of pseudowollastonite in the schorlomite-gehlenite paralava (Seryotkin et al. 2012) indicates that it was formed at temperatures not lower than 1100°C. Pliniusite crystallized from a melt locally enriched in vanadium which could be extracted from underlying phosphorites or, hypothetically, from bitumen contained in a protolith of pyrometamorphic rocks of the Hatrurim Complex.

Noteworthily, pliniusite is the second mineral containing both species-defining anions $(VO_4)^{3-}$ and $F^-$, after aradite $BaCa_6[(SiO_4)(VO_4)](VO_4)_2F$ which was also found in paralavas of the Hatrurim Complex (Galuskin et al. 2015).

~~We believe that~~ The temperature of crystallization of pliniusite in the Hatrurim paralava was significantly higher than Tolbachik fumaroles whereas low pressure and high oxidizing potential are common for both mineral-forming systems. We suggest that such conditions are favorable for the incorporation of significant amount of $V^{5+}$ into the *T* site of calcium apatite-type compounds and in general for the formation of fluorovanadate minerals.

## IMPLICATIONS

This is the peer-reviewed, final accepted version for American Mineralogist, published by the Mineralogical Society of America.
The published version is subject to change. Cite as Authors (Year) Title. American Mineralogist, in press.
DOI: https://doi.org/10.2138/am-2022-8100. http://www.minsocam.org/

Our structural data on the fluorapatite–svabite–pliniusite solid-solution system are potentially important for understanding apatite crystal chemistry in both natural and synthetic systems.Ionic radii of tetrahedrally coordinated $V^{5+}$ (0.355 Å) and $As^{5+}$ (0.335 Å) are about twice larger than that of $P^{5+}$ (0.17 Å) (Shannon, 1976). It is recognized that this difference hampers the formation of solid solutions between fluorapatite $Ca_5(PO_4)_3F$ and svabite $Ca_5(AsO_4)_3F$ or pliniusite $Ca_5(VO_4)_3F$. Moreover, the significant difference in the electron structure between vanadium (metal) and phosphorus (non-metal) atoms prevents the formation of the fluorapatite–pliniusite solid solution. Indeed, pliniusite and V-enriched Ca phosphates of the apatite group are extremely rare in nature: they were unknown before the present work. On the other hand, the apatite-type structure is relatively flexible, and the substitution of $P^{5+}$ for larger $As^{5+}$ or $V^{5+}$ in the tetrahedral *T* sites can be compensated by the distortion of the basic structural unit, a hexagonal ring formed by $TO_4$ terahedra and slightly distorted *Ca*1-centred tricapped trigonal prisms (White et al. 2005, Fig. 6). In synthetic apatites, incorporation of $V^{5+}$ can cause rotation and titling of tetrahedra accompanied by the twisting of *Ca*1-centred prisms (via changing the so-called "twist angle") (Fang et al. 2018). Besides, Boechat et al. (2020) reported the simultaneous expansion of phosphate ions and contraction of vanadate ions in the solid solution which may minimize the crystallographic disorder symmetry distortion and allow more stability to the structure in the whole composition range of solid solution.

Pliniusite was formed in two different geological formations characterized by similar physical and chemical conditions (high temperature, low pressure and high oxidizing potential) but with different mechanisms of crystallization. In paralava belonging to the pyrometamorphic Hatrurim Complex, fluorapatite containing <0.2 $(VO_4)^{3-}$ *pfu* crystallized at early stage while pliniusite with $(PO_4)^{3-}$ < 0.3 *pfu* crystallized later, probably from the residual V-enriched melt. Temperatures of crystallization of both minerals were not lower than 1100°C, i.e., the temperatures favorable to the formation of the continuous solid solution $Ca_5[(P_{1-x}V_x)O_4]_3F$, with $0 \le x \le 1$ (Deng

et al. 2015). The significant gap between phosphate and vanadate from Hatrurim paralavas (Fig. 4) is caused by their crystallization from chemically different melts. In contrast, pliniusite of fumarolic origin, though crystallized at definitely lower temperatures (500–800°C), forms a continuous solid-solution system with fluorapatite and svabite in which, however, samples close to the $Ca_5(VO_4)_3F$ end member were not found (Fig. 4).

Kinetic factors, fluctuations in gas composition and non-equilibrium conditions of crystallization of the fluorapatite–svabite–pliniusite phases in fumaroles (where gas transports some essential constituents) determine the formation of the (metastable?) solid solution with wide compositional variations in tetrahedrally coordinated components. Fluctuations in chemical composition of volcanic gas can be the major factor which determines the chemistry of this solid-solution system. Taking into account this, justly fumarolic systems can be considered as an excellent, probably the best "natural laboratory" for studies of chemical variations and mechanisms of isomorphous substitutions in high-temperature apatites.

## ACKNOWLEDGMENTS

We thank anonymous referees and Associate Editor Paolo Lotti for valuable comments. This work was supported by the Russian Science Foundation, grants nos. 19-17-00050 (mineralogical characterization and crystal structure study of pliniusite) and 20-77-00063 (chemical study of the pliniusite–svabite–fluorapatite solid-solution system). A.K. thanks for supporting in mineralogical study of Hatrurim pliniusite the National Science Centre (NCN) of Poland, Grant Preludium no. 2016/21/N/ST10/00463. The technical support by the St. Petersburg State University X-Ray Diffraction Resource Center in powder XRD study of pliniusite is acknowledged.

405 **REFERENCES CITED**

406

407 Africano, F., Van Rompaey, G., Bernard, A. and Le Guern, F. (2002) Deposition of trace elements
408 from high temperature gases of Satsuma-Iwojima volcano. Earth Planets Space, 54, 275–286.
409 Agilent Technologies (2014) CrysAlisPro Software system, version 1.171.37.35, Agilent
410 Technologies UK Ltd, Oxford, UK.
411 Aia, M.A. and Lublin, P. (1966) Blue luminescence in calcium chlorovanadates. Journal of The
412 Electrochemical Society, 113, 1331–1333.
413 Baikie, T., Mercier, P.H.J., Elcombe, M.M., Kim, J.Y., Le Page, Y., Mitchell, L.D., White, T.J., and
414 Whitfield, P.S. (2007) Triclinic apatites. Acta Crystallographica, B63, 251–256.
415 Boechat, C.B., Eon, J.-G., Rossi, A.M., de Castro Perez, C. A., and da Silva San Gilc, R.S. (2020)
416 Structure of vanadate in calcium phosphate and vanadate apatite solid solutions. Physical Chemistry
417 and Chemical Physics, 2, 4225–4230.
418 Britvin, S.N., Dolivo-Dobrovolsky, D.V., and Krzhizhanovskaya, M.G. (2017) Software for
419 processing the X-ray powder diffraction data obtained from the curved image plate detector of
420 Rigaku RAXIS Rapid II diffractometer. Zapiski Rossiiskogo Mineralogicheskogo
421 Obshchestva, 146(3), 104–107 (in Russian).
422 Burg, A., Kolodny, Y. and Lyakhovsky, V. (1999) Hatrurim-2000: The “Mottled Zone” revisited,
423 forty years later. Israel Journal of Earth Sciences, 48, 209–223.
424 Comodi, P., Yu, L., Stoppa, F. and Woolley, A. (1999) A multi-method analysis of Si, S- and REE-
425 rich apatite from a new find of kalsilite-bearing leucitite (Abruzzi, Italy). Mineralogical
426 Magazine, 63, 661–672.

427 Deng, T. Xia, Z. and Ding, H. (2015) Effect of $[PO_4]^{3-}/[VO_4]^{3-}$ substitution on the structure and
428 luminescence properties of $Ca_5[(P,V)O_4)]_3F:Eu^{3+}$ phosphors. Chemical Physics Letters, 637,
429 67–70.
430 Dong, Z. and White, T.J. (2004) Calcium-lead fluoro-vanadinite apatites. II. Equilibrium structures.
431 Acta Crystallographica, B60, 146–154.
432 Fang, Y., Page, S.J., Rees, G.J., Avdeev, M., Hanna, J.V. and White, T.J. (2018) Crystal chemistry
433 of vanadium-bearing ellestadite waste forms. Inorganic Chemistry, 57, 9122–9132.
434 Fedotov, S.A. and Markhinin, Y.K., eds. (1983) The Great Tolbachik Fissure Eruption. Cambridge
435 University Press, NY.
436 Frost, R.L., Palmer, S.J., Čejka, J., Sejkora, J., Plášil, J., Bahfenne, S. and Keeffe E.C. (2011) A
437 Raman spectroscopic study of the different vanadate groups in solid-state compounds –model
438 case:mineral phases vésigniéite $[BaCu_3(VO_4)_2(OH)_2]$ and volborthite $[Cu_3V_2O_7(OH)_2\cdot 2H_2O]$.
439 Journal of Raman Spectroscopy, 42, 1701–1710.
440 Frost, R.L., López, A., Scholz, R., Lana, C. and Xi, Y. (2015) A Raman spectroscopic study of the
441 arsenate mineral chenevixite $Cu_2Fe_2^{3+}(AsO_4)_2(OH)_4\cdot H_2O$. Spectrochimica Acta Part A:
442 Molecular and Biomolecular Spectroscopy, 135, 192–197.
443 Galuskin, E.V., Gfeller, F., Galuskina, I.O., Pakhomova, A., Armbruster, T., Vapnik, Y., Włodyka,
444 R., Dzierżanowski, P. and Murashko, M. (2015) New minerals with a modular structure
445 derived from hatrurite from the pyrometamorphic Hatrurim Complex. Part II. Zadovite,
446 $BaCa_6[(SiO_4)(PO_4)](PO_4)_2F$ and aradite, $BaCa_6[(SiO_4)(VO_4)](VO_4)_2F$, from paralavas of the
447 Hatrurim Basin, Negev Desert, Israel. Mineralogical Magazine, 79, 1073–1087.
448 Galuskina, I.O., Vapnik, Y., Lazic, B., Armbruster, T., Murashko, M. and Galuskin, E.V. (2014)
449 Harmunite $CaFe_2O_4$: A new mineral from the Jabel Harmun, West Bank, Palestinian
450 Autonomy, Israel. American Mineralogist, 99, 965–975.

Gross, S. (1977) The mineralogy of the Hatrurim Formation, Israel. Geological Survey of Israel Bulletin, 70, 1–80.

Kohn, M.J., Rakovan, J. and Hughes, J.M., eds. (2002) Phosphates: Geochemical, Geobiological, and Matrerials Importance. Reviews in Mineralogy and Geochemistry, 48, issue 1.

Kreidler, E.R. and Hummel, F.A. (1970) The crystal chemistry of apatite: structure fields of fluor- and chlorapatite. American Mineralogist, 55, 170–184.

Krzątała, A., Krüger, B., Galuskina, I., Vapnik, Y. and Galuskin, E. (2020) Walstromite, $BaCa_2(Si_3O_9)$, from rankinite paralava within gehlenite hornfels of the Hatrurim Basin, Negev Desert, Israel. Minerals, 10, 407.

Meniaylov, I.A., Nikitina, L.P. and Shapar', V.N. (1980) Geochemical Features of Exhalations of the Great Tolbachik Fissure Eruption. Nauka Publishing, Moscow (in Russian).

Novikov, I., Vapnik, Y. and Safonova, I. (2013) Mud volcano origin of the Mottled Zone, South Levant. Geoscience Frontiers, 4, 597–619.

Pasero, M., Kampf, A.R., Ferraris, C., Pekov, I.V., Rakovan, J. and White, T.J. (2010) Nomenclature of the apatite supergroup minerals. European Journal of Mineralogy, 22, 163–179.

Pekov, I.V., Koshlyakova, N.N., Zubkova, N.V., Lykova, I.S., Britvin, S.N., Yapaskurt, V.O., Agakhanov, A.A., Shchipalkina, N.V., Turchkova, A.G., and Sidorov, E.G. (2018) Fumarolic arsenates – a special type of arsenic mineralization. European Journal of Mineralogy, 30, 305–322.

Pekov, I.V., Agakhanov, A.A., Zubkova, N.V., Koshlyakova, N.N., Shchipalkina, N.V., Sandalov, F.D., Yapaskurt, V.O., Turchkova, A.G. and Sidorov E.G. (2020) Oxidizing-type fumaroles of the Tolbachik Volcano, a mineralogical and geochemical unique. Russian Geology and Geophysics, 61(5-6), 675–688.

475 Seryotkin, Yu.V., Sokol, E.V. and Kokh, S. (2012) Natural pseudowollastonite: Crystal structure,
476 associated minerals, and geological context. Lithos, 134-135, 75–90.
477 Shannon, R.D. (1976) Revised effective ionic radii and systematic studies of interatomic distances
478 in halides and chalcogenides. Acta Crystallographica, A32, 751–767.
479 Sharygin, V.V., Vapnik, Y., Sokol, E.V., Kamenetsky, V.S. and Shagam, R. (2006) Melt inclusions
480 in minerals of schorlomite-rich veins of the Hatrurim Basin, Israel: composition and
481 homogenization temperatures. Asian Current Research on Fluid Inclusions, 189–192.
482 Shchipalkina N.V., Pekov I.V., Koshlyakova N.N., Britvin S.N., Zubkova N.V., Varlamov D.A.,
483 Sidorov E.G. (2020) Unusual silicate mineralization in fumarolic sublimates of the Tolbachik
484 volcano, Kamchatka, Russia – Part 1: Neso-, cyclo-, ino- and phyllosilicates. European Journal
485 of Mineralogy, 32, 101–119.
486 Sheldrick, G.M. (2008) A short history of SHELX. Acta Crystallographica, A64, 112–122.
487 Symonds, R.B. and Reed, M.H. (1993) Calculation of multicomponent chemical equilibria in gas-
488 solid-liquid systems: calculation methods, thermochemical data, and applications to studies of
489 high-temperature volcanic gases with examples from Mount St. Helens. American Journal of
490 Science, 293, 758–864.
491 The New IMA List of Minerals. Updated: May 2021 (2021). http://cnmnc.main.jp
492 Vapnik, Y., Sharygin, V.V., Sokol, E.V. and Shagam, R. (2007) Paralavas in a combustion
493 metamorphic complex: Hatrurim Basin, Israel. In: Geology of Coal Fires: Case Studies from
494 Around the World; Geological Society of America, 18, 133–153.
495 White, T., Ferraris, C., Kim, J. and Srinivasan, M. (2005) Apatite – an adaptive framework
496 structure. In: Micro- and Mesoporous Mineral Phases (G. Ferraris and S. Merlino, eds.).
497 Reviews in Mineralogy and Geochemistry, 57, 307–402.

498 Zelenski, M.E., Zubkova, N.V., Pekov, I.V., Boldyreva, M.M., Pushcharovsky, D.Yu. and
499 Nekrasov, A.N. (2011) Pseudolyonsite, $Cu_3(VO_4)_2$, a new mineral species from the Tolbachik
500 volcano, Kamchatka Peninsula, Russia. European Journal of Mineralogy, 23, 475–481.

501 **Figure captions**

502

503 **Figure 1.** SEM/BSE image of crystals of pliniusite (1) on hematite crystal crust (2) with baryte (3).
504 The holotype specimen is from Mountain 1004, Tolbachik volcano, Kamchatka, Russia.

505

506 **Figure 2.** Whitish open-work aggregates of prismatic pliniusite crystals with yellow diopside on
507 crust consisting of iron-black hematite which covers basalt scoria. The holotype specimen is from
508 Mountain 1004, Tolbachik volcano. FOV width: 2.15 mm. Photo: I.V. Pekov and A.V. Kasatkin.

509

510 **Figure 3.** Pliniusite in the cotype specimen from Nahal Morag, Hatrurim Basin, Israel. A – general
511 view of coarse-grained paralava: reddish-brown – andradite-schrolomite series garnet, light yellow-
512 brown – melilite, colourless – rankinite, wollastonite and cuspidine. B – inclusion of Ba- and $V^{5+}$-
513 bearing minerals in rankinite (Rnk); fragment magnified in C is shown in the frame. C – elongated
514 crystals of pliniusite (Pls) in association with walstromite (Wls), gurimite (Gur), tenorite (Tnr),
515 cuspidine (Cus), rankinite (Rnk), wollastonite (Wo), and secondary Ca-hydrosilicates (HSi). B and
516 C are SEM/BSE images of polished sections.

517

518 **Figure 4.** Ratios of major tetrahedrally coordinated constituents (*T*) in minerals of the pliniusite–
519 svabite–fluorapatite solid-solution system.

520

521 **Figure 5.** Raman spectra of pliniusite from (a) Nahal Morag, Hatrurim Basin (cotype) and (b)
522 Mountain 1004, Tolbachik volcano (holotype).

523

524 **Figure 6.** Crystal structure of pliniusite (space group $P6_3/m$) projected down the *c*-axis. Black lines
525 outline the unit cell.

526

This is the peer-reviewed, final accepted version for American Mineralogist, published by the Mineralogical Society of America.
The published version is subject to change. Cite as Authors (Year) Title. American Mineralogist, in press.
DOI: https://doi.org/10.2138/am-2022-8100. http://www.minsocam.org/

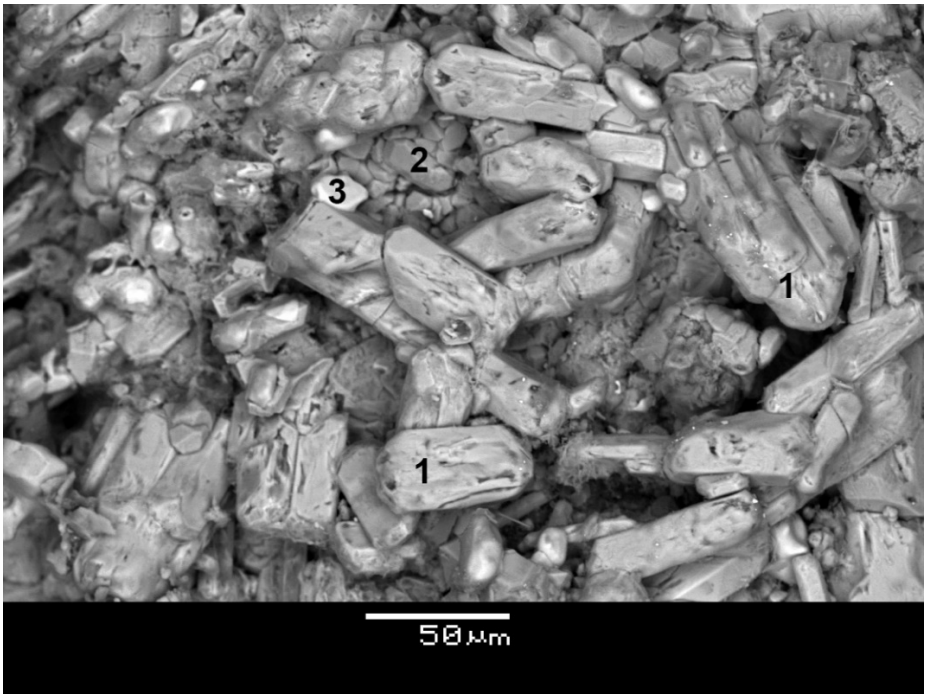


527

528 **Figure 1**

529

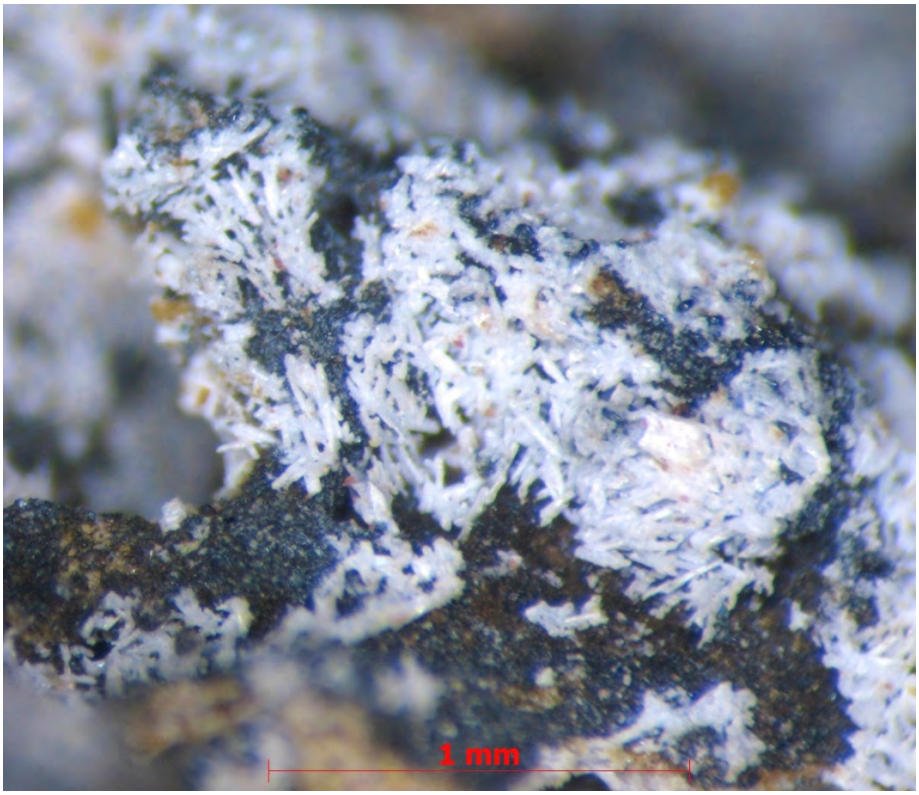


530

531 **Figure 2**

532

533

This is the peer-reviewed, final accepted version for American Mineralogist, published by the Mineralogical Society of America.
The published version is subject to change. Cite as Authors (Year) Title. American Mineralogist, in press.
DOI: https://doi.org/10.2138/am-2022-8100. http://www.minsocam.org/

534

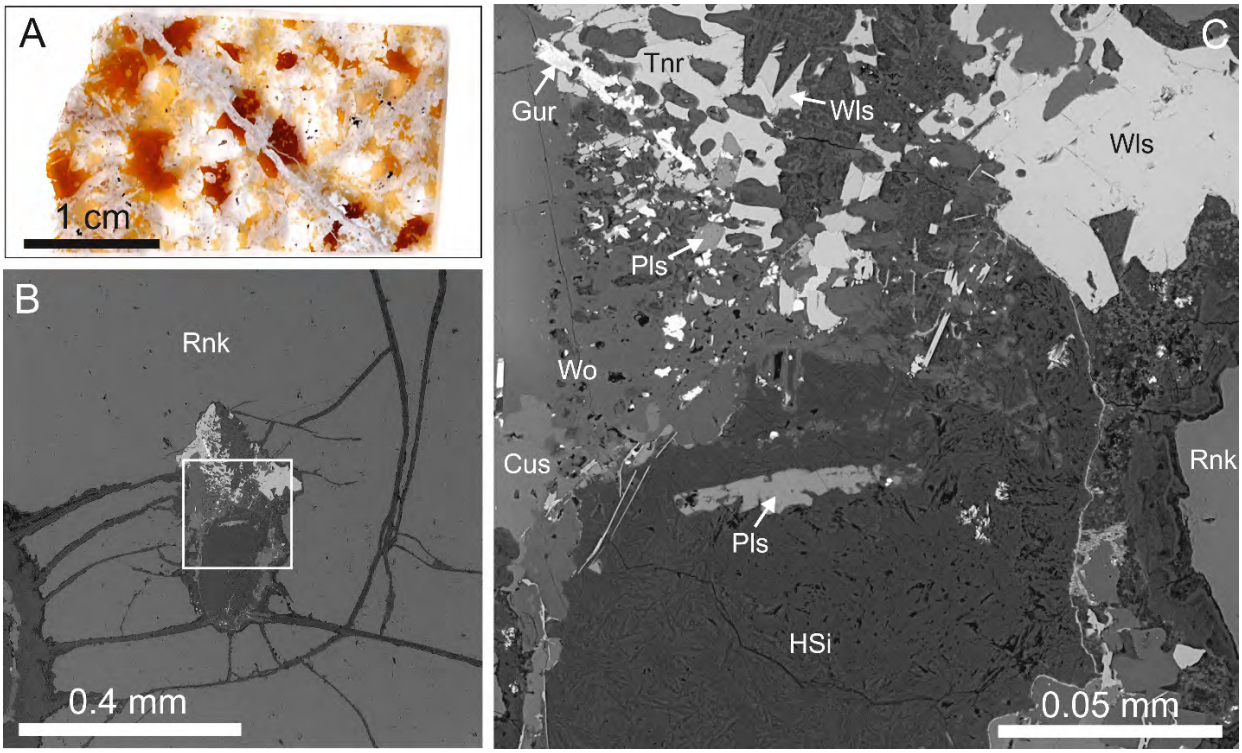


535

536 **Figure 3**

537

This is the peer-reviewed, final accepted version for American Mineralogist, published by the Mineralogical Society of America.
The published version is subject to change. Cite as Authors (Year) Title. American Mineralogist, in press.
DOI: https://doi.org/10.2138/am-2022-8100. http://www.minsocam.org/

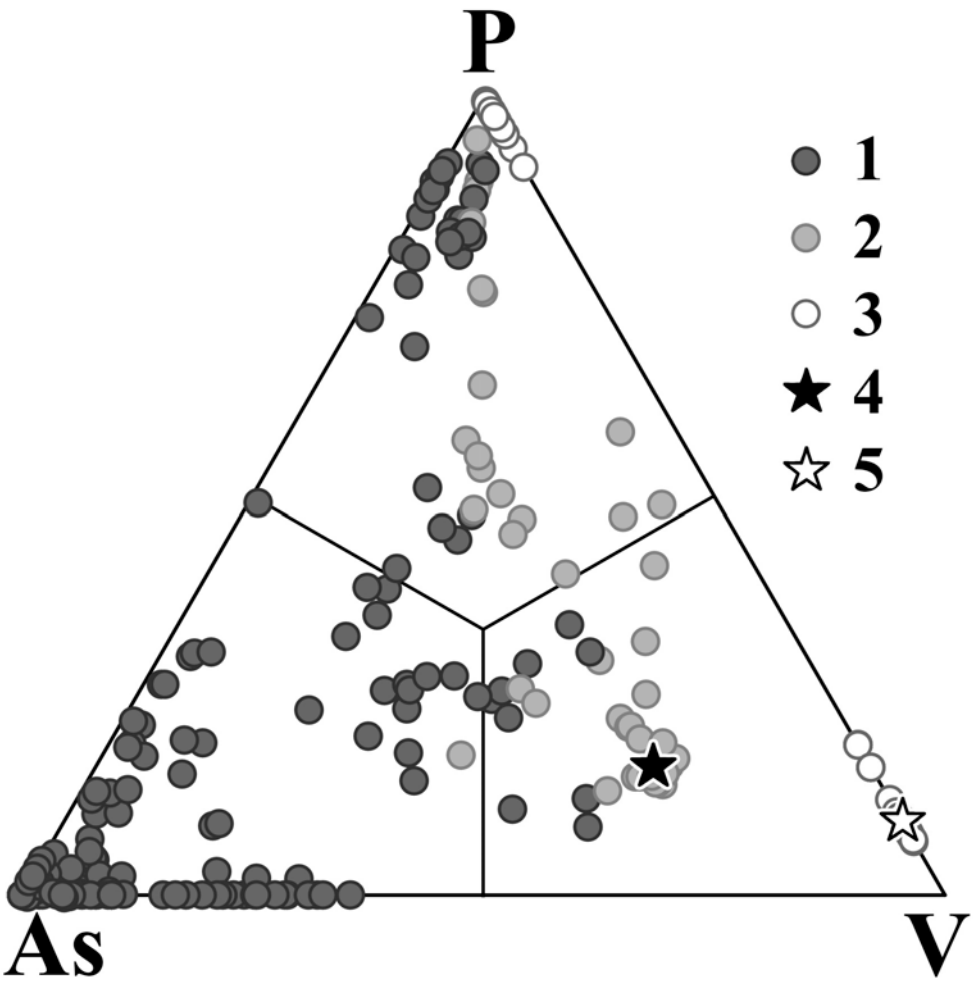


538

539 **Figure 4**

540

This is the peer-reviewed, final accepted version for American Mineralogist, published by the Mineralogical Society of America.
The published version is subject to change. Cite as Authors (Year) Title. American Mineralogist, in press.
DOI: https://doi.org/10.2138/am-2022-8100. http://www.minsocam.org/

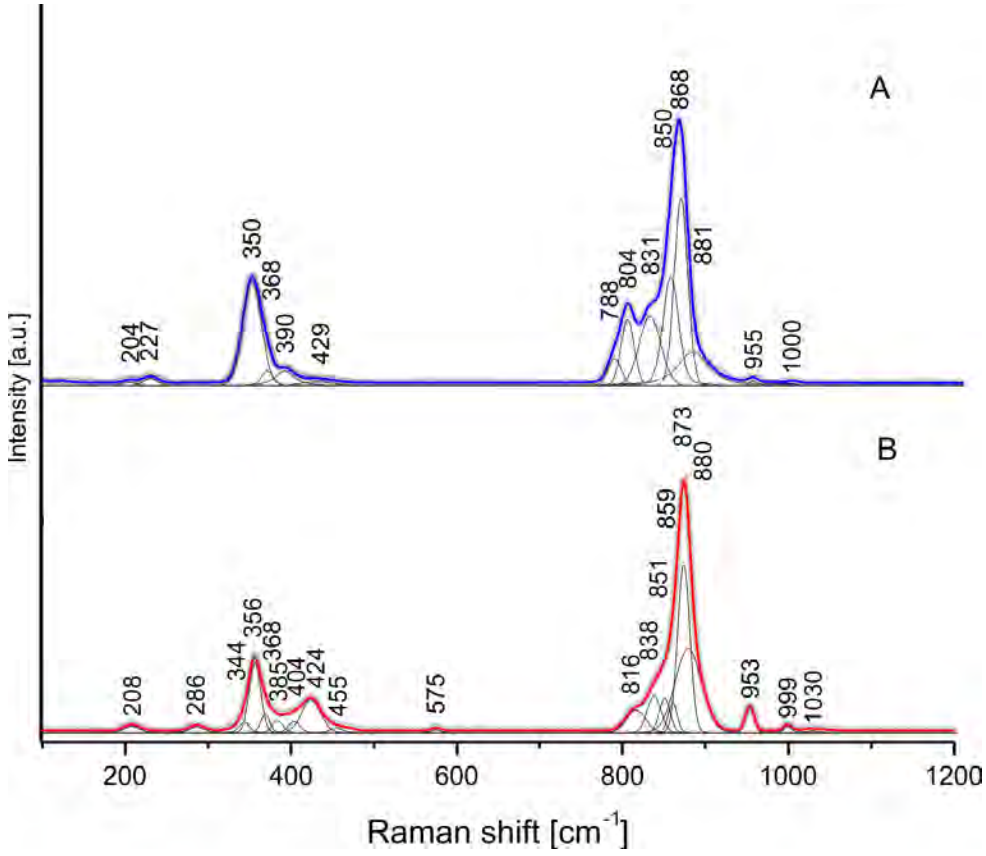


541

542 **Figure 5**

543

This is the peer-reviewed, final accepted version for American Mineralogist, published by the Mineralogical Society of America.
The published version is subject to change. Cite as Authors (Year) Title. American Mineralogist, in press.
DOI: https://doi.org/10.2138/am-2022-8100. http://www.minsocam.org/

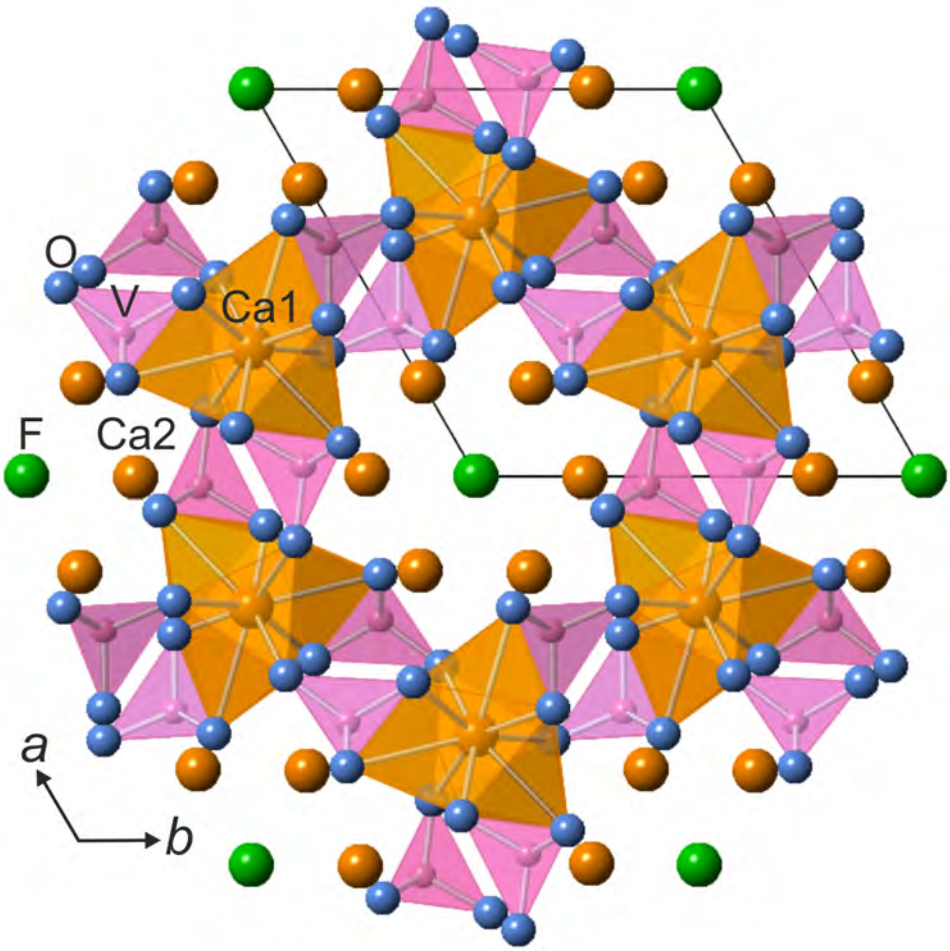


544

545 **Figure 6**

This is the peer-reviewed, final accepted version for American Mineralogist, published by the Mineralogical Society of America.
The published version is subject to change. Cite as Authors (Year) Title. American Mineralogist, in press.
DOI: https://doi.org/10.2138/am-2022-8100. http://www.minsocam.org/

546 **Tables**

547

548 **Table 1**. Chemical composition of minerals of the pliniusite–fluorapatite–svabite solid-solution system.

| No. | 1 | 2 | 3 | 4 | 5 | 6 | 7 | 8 | 9 |
|---|---|---|---|---|---|---|---|---|---|
| Locality | Mt. 1004 | N. M. | N. M. | Mt. 1004 | Mt. 1004 | Arsen. | Mt. 1004 | Mt. 1004 | Mt. 1004 |
| Mineral | Pln (holotype) | Pln (cotype) | Pln | Pln | Pln | Pln | FAp | FAp | FAp |
| | | | wt. % | | | | | | |
| $Na_2O$ | 0.33 (0.00 – 0.41) | 0.26 (0.13 – 0.37) | 0.20 | 0.37 | 0.04 | 0.32 | 0.34 | 0.39 | 0.23 |
| $K_2O$ | 0.01 (0.00 – 0.02) | | 0.05 | | | | | | |
| CaO | 48.04 (47.57 – 48.50) | 45.92 (45.25 – 46.67) | 45.10 | 48.21 | 47.81 | 46.40 | 48.13 | 49.79 | 48.81 |
| SrO | 0.58 (0.49 – 0.69) | 2.05 (1.94 – 2.16) | 2.01 | 0.50 | 0.45 | 0.69 | 0.49 | 0.61 | 0.38 |
| BaO | | 2.14 (1.81 – 2.48) | 2.36 | | | | | | |
| FeO | 0.26 (0.00 – 0.52) | | 0.18 | 0.25 | 0.12 | | 0.19 | 0.12 | 0.35 |
| $SiO_2$ | 0.94 (0.67 – 1.19) | 0.34 (0.22 – 0.65) | 0.22 | 0.85 | 1.18 | 1.05 | 0.78 | 0.46 | 0.96 |
| $P_2O_5$ | 5.63 (4.84 – 7.44) | 3.13 (2.57 – 4.28) | 2.75 | 5.28 | 8.93 | 8.56 | 7.44 | 18.52 | 14.31 |
| $V_2O_5$ | 27.04 (25.01 – 27.90) | 41.03 (40.20 – 41.54) | 42.22 | 27.59 | 18.16 | 17.23 | 25.00 | 21.73 | 17.61 |
| $As_2O_5$ | 13.26 (11.67 – 14.97) | | | 12.77 | 18.48 | 20.76 | 13.57 | 3.82 | 12.02 |
| $SO_3$ | 1.73 (1.48 – 1.93) | 0.95 (0.62 – 1.36) | 0.75 | 1.73 | 1.22 | 1.81 | 1.66 | 1.19 | 1.62 |
| F | 3.46 (3.18 – 3.67) | 1.65 (1.48 – 1.80) | 1.58 | 3.18 | 3.01 | 2.82 | 3.33 | 3.53 | 3.41 |
| Cl | | 2.07 (1.79 – 2.26) | 2.28 | | 0.07 | 1.13 | | | |
| –O=F+Cl | 1.46 | 1.16 | 1.18 | 1.34 | 1.28 | 1.44 | 1.40 | 1.49 | 1.44 |
| Total | 99.82 | 98.38 | 98.52 | 99.39 | 98.19 | 99.33 | 99.53 | 98.67 | 98.26 |

549

550

This is the peer-reviewed, final accepted version for American Mineralogist, published by the Mineralogical Society of America.
The published version is subject to change. Cite as Authors (Year) Title. American Mineralogist, in press.
DOI: https://doi.org/10.2138/am-2022-8100. http://www.minsocam.org/

551
552 **Table 1** (continued).

| No. | 1 | 2 | 3 | 4 | 5 | 6 | 7 | 8 | 9 |
|---|---|---|---|---|---|---|---|---|---|
| Locality | Mt. 1004 | Nahal Morag | N. M. | Mt. 1004 | Mt. 1004 | Arsen. | Mt. 1004 | Mt. 1004 | Mt. 1004 |
| Mineral | Pln (holotype) | Pln (cotype) | Pln | Pln | Pln | Pln | FAp | FAp | FAp |
| | formula calculated on the basis of 13 anions (O+F+Cl) | | | | | | | | |
| Na | 0.06 | 0.05 | 0.04 | 0.07 | - | 0.06 | 0.06 | 0.07 | 0.04 |
| K | - | | - | | | | | | |
| Ca | 4.87 | 4.77 | 4.72 | 4.90 | 4.94 | 4.82 | 4.88 | 4.85 | 4.90 |
| Sr | 0.03 | 0.11 | 0.11 | 0.03 | 0.03 | 0.04 | 0.03 | 0.03 | 0.02 |
| Ba | | 0.08 | 0.09 | | | | | | |
| Fe | 0.02 | | 0.01 | 0.02 | - | | 0.01 | - | 0.03 |
| Si | 0.09 | 0.03 | 0.02 | 0.08 | 0.11 | 0.10 | 0.07 | 0.04 | 0.09 |
| P | 0.45 | 0.26 | 0.23 | 0.42 | 0.73 | 0.70 | 0.60 | 1.43 | 1.13 |
| V | 1.69 | 2.63 | 2.72 | 1.73 | 1.16 | 1.10 | 1.56 | 1.31 | 1.09 |
| As | 0.66 | | | 0.63 | 0.93 | 1.05 | 0.67 | 0.18 | 0.59 |
| S | 0.12 | 0.07 | 0.05 | 0.12 | 0.09 | 0.13 | 0.12 | 0.08 | 0.11 |
| F | 1.04 | 0.51 | 0.49 | 0.95 | 0.92 | 0.86 | 1.00 | 1.01 | 1.01 |
| Cl | | 0.34 | 0.38 | | 0.01 | 0.19 | | | |
| O | 11.99 | 12.05 | 12.11 | 12.01 | 12.05 | 12.10 | 12.03 | 12.04 | 12.02 |
| $\sum M$ | 4.98 | 5.01 | 4.97 | 5.02 | 4.97 | 4.92 | 4.98 | 4.95 | 4.99 |
| $\sum T$ | 3.01 | 2.99 | 3.02 | 2.98 | 3.02 | 3.08 | 3.02 | 3.04 | 3.01 |
| $\sum$F+Cl | 1.04 | 0.85 | 0.87 | 0.95 | 0.93 | 1.05 | 1.00 | 1.01 | 1.01 |

553
554

This is the peer-reviewed, final accepted version for American Mineralogist, published by the Mineralogical Society of America.
The published version is subject to change. Cite as Authors (Year) Title. American Mineralogist, in press.
DOI: https://doi.org/10.2138/am-2022-8100. http://www.minsocam.org/

555
556 **Table 1** (continued).

| No. | 10 | 11 | 12 | 13 | 14 | 15 | 16 | 17 | 18 | 19 |
|---|---|---|---|---|---|---|---|---|---|---|
| Locality | Mt. 1004 | N. M. | N. M. | Arsen. | Arsen. | Arsen. | Arsen. | Arsen. | Arsen. | Arsen. |
| Mineral | FAp | FAp | FAp | FAp | Svb | Svb | Svb | Svb | Svb | Svb |
| | | | | | wt. % | | | | | |
| $Na_2O$ | 0.27 | 0.01 | | 0.59 | | 0.68 | 0.40 | 0.66 | 0.40 | 0.78 |
| CaO | 49.59 | 53.83 | 53.52 | 53.16 | 44.78 | 42.67 | 45.47 | 46.06 | 44.40 | 43.80 |
| SrO | 0.35 | 0.95 | 1.02 | 0.09 | | 0.19 | 0.27 | 0.18 | | |
| BaO | | 0.15 | 0.83 | | | | | | | |
| MnO | | 0.04 | | | | 0.29 | 0.16 | | | |
| FeO | 0.37 | 0.13 | | | | | | | | 0.16 |
| $SiO_2$ | 1.17 | 0.85 | 2.60 | 0.22 | | 0.25 | 3.51 | 0.24 | 0.17 | 0.10 |
| $P_2O_5$ | 19.18 | 39.39 | 36.19 | 37.20 | | 0.18 | 4.17 | 9.36 | 4.04 | 0.55 |
| $V_2O_5$ | 10.60 | 2.02 | 0.80 | 0.06 | 13.94 | 3.88 | 3.45 | 1.03 | 0.66 | 0.49 |
| $As_2O_5$ | 13.61 | | | 5.96 | 37.29 | 47.71 | 33.38 | 40.80 | 47.00 | 51.63 |
| $SO_3$ | 1.99 | 0.40 | 1.38 | 0.49 | 0.91 | 1.48 | 5.05 | 1.16 | 0.80 | 1.86 |
| $CrO_3$ | | 0.38 | 0.03 | | | | | | | |
| F | 3.89 | 3.28 | 4.00 | 4.02 | 2.00 | 2.22 | 2.33 | 3.05 | 3.01 | 3.22 |
| Cl | | 0.01 | | 0.20 | 2.41 | 1.53 | 1.71 | 0.44 | 0.48 | 0.06 |
| –O=F+Cl | 1.64 | 1.38 | 1.68 | 1.74 | 1.38 | 1.28 | 1.36 | 1.38 | 1.38 | 1.37 |
| Total | 99.38 | 100.06 | 98.69 | 100.25 | 99.95 | 99.80 | 98.54 | 101.60 | 99.58 | 101.28 |

557
558

This is the peer-reviewed, final accepted version for American Mineralogist, published by the Mineralogical Society of America.
The published version is subject to change. Cite as Authors (Year) Title. American Mineralogist, in press.
DOI: https://doi.org/10.2138/am-2022-8100. http://www.minsocam.org/

559
560 **Table 1** (continued).

| No. | 10 | 11 | 12 | 13 | 14 | 15 | 16 | 17 | 18 | 19 |
|---|---|---|---|---|---|---|---|---|---|---|
| Locality | Mt. 1004 | N. M. | N. M. | Arsen. | Arsen. | Arsen. | Arsen. | Arsen. | Arsen. | Arsen. |
| Mineral | FAp | FAp | FAp | FAp | Svb | Svb | Svb | Svb | Svb | Svb |
| formula calculated on the basis of 13 anions (O+F+Cl) | | | | | | | | | | |
| Na | 0.05 | - | | 0.10 | | 0.14 | 0.08 | 0.13 | 0.08 | 0.16 |
| Ca | 4.88 | 4.88 | 4.93 | 4.88 | 4.96 | 4.79 | 4.85 | 4.83 | 4.91 | 4.82 |
| Sr | 0.02 | 0.05 | 0.05 | - | | 0.01 | 0.01 | 0.01 | | |
| Ba | | - | 0.03 | | | | | | | |
| Mn | | - | | | | 0.03 | 0.01 | | | |
| Fe | 0.03 | - | | | | | | | | 0.01 |
| Si | 0.11 | 0.07 | 0.22 | 0.02 | | 0.03 | 0.35 | 0.02 | 0.02 | 0.01 |
| P | 1.49 | 2.82 | 2.63 | 2.70 | | 0.02 | 0.35 | 0.78 | 0.35 | 0.05 |
| V | 0.64 | 0.11 | 0.05 | - | 0.95 | 0.27 | 0.23 | 0.07 | 0.04 | 0.03 |
| As | 0.65 | | | 0.27 | 2.02 | 2.61 | 1.74 | 2.09 | 2.54 | 2.77 |
| S | 0.14 | 0.03 | 0.09 | 0.03 | 0.07 | 0.12 | 0.38 | 0.08 | 0.06 | 0.14 |
| Cr | | 0.03 | - | | | | | | | |
| F | 1.13 | 0.88 | 1.09 | 1.09 | 0.65 | 0.73 | 0.73 | 0.94 | 0.98 | 1.05 |
| Cl | | - | | 0.03 | 0.42 | 0.27 | 0.29 | 0.07 | 0.08 | 0.01 |
| O | 11.98 | 12.10 | 11.87 | 11.92 | 12.05 | 12.03 | 12.03 | 12.01 | 11.97 | 11.98 |
| $\sum M$ | 4.98 | 4.93 | 5.01 | 4.98 | 4.96 | 4.97 | 4.95 | 4.97 | 4.99 | 4.99 |
| $\sum T$ | 3.03 | 3.06 | 2.99 | 3.02 | 3.04 | 3.05 | 3.05 | 3.04 | 3.01 | 3.00 |
| $\sum$F+Cl | 1.13 | 0.88 | 1.09 | 1.12 | 1.07 | 1.00 | 1.02 | 1.01 | 1.06 | 1.06 |

561
562 Pliniusite, fluorapatite and svabite are labeled as Pln, FAp and Svb, respectively. The localities are labeled as: Mt. 1004 – Southern fumarole
563 field at Mountain 1004, Tolbachik volcano (Nos. 1, 4–7, 9, 10, 12); N. M. – Nahal Morag, Hatrurim Basin (Nos. 2, 3, 15, 17); Arsen. –
564 fumarole Arsenatnaya, Tolbachik (Nos. 8, 11, 13, 14, 16, 18, 19).
565 $\Sigma M$ = Na+K+Ca+Sr+Ba+Mn+Fe, $\Sigma T$ = Si+P+V+As+S+Cr. Empty cell means that the content of a constituent is below the detection limit
566 and dash means 0.00 *apfu* (for minor admixtures). Nos. 1 and 2: average values for eight and five spot analyses, respectively; ranges are
567 given in parentheses.

This is the peer-reviewed, final accepted version for American Mineralogist, published by the Mineralogical Society of America.
The published version is subject to change. Cite as Authors (Year) Title. American Mineralogist, in press.
DOI: https://doi.org/10.2138/am-2022-8100. http://www.minsocam.org/

568 **Table 2.** Powder X-ray diffraction data (*d* in Å) of the holotype pliniusite.

| $I_{obs}$ | $d_{obs}$ | $I_{calc}$* | $d_{calc}$** | *h k l* |
|---|---|---|---|---|
| 11 | 8.32 | 10 | 8.295 | 100 |
| 5 | 5.347 | 4 | 5.334 | 101 |
| 7 | 4.807 | 4 | 4.789 | 110 |
| 3 | 4.163 | 2 | 4.147 | 200 |
| **27** | **3.958** | 20 | 3.946 | 111 |
| 4 | 3.575 | 3 | 3.564 | 201 |
| **33** | **3.488** | 40 | 3.483 | 002 |
| 7 | 3.217 | 7 | 3.211 | 102 |
| 14 | 3.148 | 13 | 3.135 | 210 |
| **100** | **2.869** | 100 | 2.859 | 211 |
| **35** | **2.823** | 42 | 2.817 | 112 |
| **58** | **2.776** | 55 | 2.765 | 300 |
| **25** | **2.674** | 27 | 2.667 | 202 |
| 6 | 2.579 | 5 | 2.570 | 301 |
| 3 | 2.337 | 3 | 2.330 | 212 |
| 16 | 2.310 | 15 | 2.300 | 130 |
| 7 | 2.274 | 8 | 2.264 | 221 |
| 8 | 2.194 | 9 | 2.184 | 311 |
| 1 | 2.082 | 1 | 2.074 | 400 |
| 2 | 2.031 | 2 | 2.026 | 203 |
| **19** | **1.980** | 28 | 1.973 | 222 |
| 4 | 1.926 | 6 | 1.920 | 132 |
| 3 | 1.912 | 3 | 1.903 | 230 |
| **23** | **1.871** | 38 | 1.866 | 213 |
| 16 | 1.844 | 15 | 1.836 | 321 |
| 7 | 1.818 | 10 | 1.810 | 140 |
| 6 | 1.788 | 9 | 1.782 | 402 |
| 2 | 1.759 | 2 | 1.752 | 141 |
| 6 | 1.745 | 18 | 1.741 | 004 |
| 9 | 1.676 | 15 | 1.670 | 232 |
| 2 | 1.665 | 2 | 1.659 | 500 |
| 3 | 1.639 | 6 | 1.634 | 133 |
| 1 | 1.619 | 1 | 1.614 | 501 |
| 1 | 1.606 | 1 | 1.606 | 142 |
| 4 | 1.575 | 6 | 1.568 | 240 |
| 3 | 1.563 | 5 | 1.556 | 331 |
| 4 | 1.536 | 6 | 1.529 | 421 |
| 2 | 1.526 | 3 | 1.522 | 124 |
| 9 | 1.504 | 17 | 1.498 | 502 |
| 2 | 1.489 | 2 | 1.490 | 150 |
| 8 | 1.477 | 12, 6 | 1.474, 1.472 | 304, 233 |
| 5 | 1.463 | 8 | 1.457 | 511 |
| 2 | 1.433 | 2, 3 | 1.429, 1.428 | 242, 413 |
| 1 | 1.392 | 1 | 1.388 | 134 |

This is the peer-reviewed, final accepted version for American Mineralogist, published by the Mineralogical Society of America.
The published version is subject to change. Cite as Authors (Year) Title. American Mineralogist, in press.
DOI: https://doi.org/10.2138/am-2022-8100. http://www.minsocam.org/

| | | | | |
|---|---|---|---|---|
| 2 | 1.375 | 4 | 1.370 | 152 |
| 4 | 1.344 | 8, 1 | 1.338, 1.338 | 341, 115 |
| 2 | 1.335 | 4 | 1.328 | 250 |
| 3 | 1.304 | 3, 7 | 1.305, 1.299 | 521, 243 |
| 1 | 1.289 | 2 | 1.285 | 234 |
| 4 | 1.276 | 8 | 1.273 | 125 |
| 3 | 1.272 | 3, 4 | 1.270, 1.265 | 342, 610 |
| 5 | 1.259 | 7, 5 | 1.255, 1.254 | 144, 513 |
| 3 | 1.247 | 7 | 1.241 | 252 |
| 2 | 1.204 | 2, 3 | 1.204, 1.201 | 225, 504 |

*For the calculated pattern, only reflections with intensities ≥1 are given; **calculated with the unit-cell parameters from single-crystal XRD data. The strongest reflections are marked in bold.

**Table 3.** Selected bond lengths (Å) of the holotype pliniusite.

| | | | |
|---|---|---|---|
| *T* – O(3) | 1.625(2) x 2 | Ca2 – F | 2.3248(8) |
| - O(2) | 1.627(3) | - O(3) | 2.347(2) x 2 |
| - O(1) | 1.647(3) | - O(1) | 2.398(3) |
| <*T*-O> | 1.631 | - O(3) | 2.497(2) x 2 |
| | | - O(2) | 2.744(3) |
| Ca1 – O(2) | 2.395(2) x 3 | <Ca-F/O> | 2.451 |
| - O(1) | 2.482(2) x 3 | | |
| - O(3) | 2.874(2) x 3 | | |
| <Ca-O> | 2.584 | | |